Chapter 2

Pathological Diagnosis with Scanning Acoustic Microscopy and Photoacoustic Microscopy

Bukem Tanoren

Department of Physics, Bebek, 34342, Istanbul, Turkey

Email: bukem.bilen1@boun.edu.tr

1. Definition

Ultrasound has proved its diagnostic value through last five decades. For the observation of soft tissue, ultrasound (US) imaging has become very popular, since it has high axial and lateral resolutions of approximately 20-100 μm and a good penetration depth of approximately 5 mm. US imaging has also low cost, however, it can only provide information about the morphology. Scanning acoustic microscopy (SAM) is an imaging tool which uses high frequency ultrasound and provides morphological and mechanical information about the specimen simultaneously at microscopic levels. Photoacoustic microscopy (PAM) is a well-known imaging modality that combines optical and ultrasound imaging and obtains chemical and morphology information with a good penetration depth and with a micrometer resolution. Detection of micro-meter sized formations within tissues or cells with a good penetration depth is possible with a combined SAM and PAM system, which uses ultrasound waves rather than a system using ionizing radiation.

Keywords: Scanning Acoustic Microscopy; Photoacoustic Microscopy; Acoustic Impedance; Sound Speed; 2D Imaging; 3D Imaging

2. History

With no harm created on humans, low cost ultrasound imaging is conventionally used for the observation of soft tissue, however, it can only provide morphological information. Besides, the signal detection capability has to be increased for the detection of micro-meter sized formations, since high echo signals from such small surfaces are not available [1]. These disabilities have been overcome by combining ultrasound with photoacoustic imaging and the detection of lipid-laden plaque was achieved by providing both morphological

and lipid-specific chemical information about the human coronary artery [2]. Similarly, intravascular implementation of photoacoustic imaging provided characterization of spatial and quantitative features of lipid-rich aortic plaques [3]. In photoacoustic microscopy (PAM) typically, nanosecond lasers excite the tissue, and absorbed photons lead to pressure waves via thermoelastic expansion [4]. Ultrasonic transducers capture the emerged pressure waves and produce the map of optical absorbers located within the tissue. Since ultrasonic waves scatter less in biological tissue as opposed to visible portion of electromagnetic spectrum, whole body imaging is possible with a tomographic approach [5]. To increase the penetration even further, lasers operating in the near infrared region are preferred for excitation where tissue is relatively transparent. Besides, targeted contrast agents are used to enhance the contrast of the micro-meter sized formations within tissues for early detection and therapy [6,7].

Scanning acoustic microscopy (SAM) is an imaging modality giving information about the morphology and the mechanical properties of the specimen simultaneously at microscopic levels. Focused high-frequency ultrasound signals are used to identify the elastic properties of biological tissues. One advantage of SAM over other imaging techniques is no need for a special staining. Besides, capture of an image of an area of around 5 mm x 5 mm is possible in a couple of minutes. Either the speed of sound (SOS) through tissues [8-17] or acoustic impedance of samples [18,19] can be calculated by SAM and two-dimensional distributions are mapped. Similarly, cells and organelles can be resolved by acoustic microscopy using higher frequencies of 100 to 1200 MHz [20-27]. Combining SAM and PAM will result in obtaining characterization of tissues in 3 dimensions with a micrometer resolution.

3. Scanning Acoustic Microscopy

SAM is mainly composed of a transducer with an ultrasonic lens, a pulser/receiver, an oscilloscope and a computer with a display monitor. Transducer, mounted on an X-Y stage controlled by the computer, generates acoustic waves and also receives the reflected waves. Medical transducers use piezoelectric crystals to generate and receive ultrasound and in most of the ultrasound imaging systems, transducers having resonant frequencies in the range of 1-20 MHz are plugged. The frequency has an influence on the image quality and therefore resolution. A matching layer is necessary for acoustic pulse to be transmitted, without a loss, to the tissue or cell under investigation. More generally, water is chosen to be the coupling medium between the ultrasonic lens and the specimen. Oscilloscope is used to analyze the signals reflected from the surface of the specimen and received by the transducer. Finally, the two-dimensional maps of the samples are constructed using either sound speed mode (**Figure 1**) or acoustic impedance mode (**Figure 2**) of the microscope.
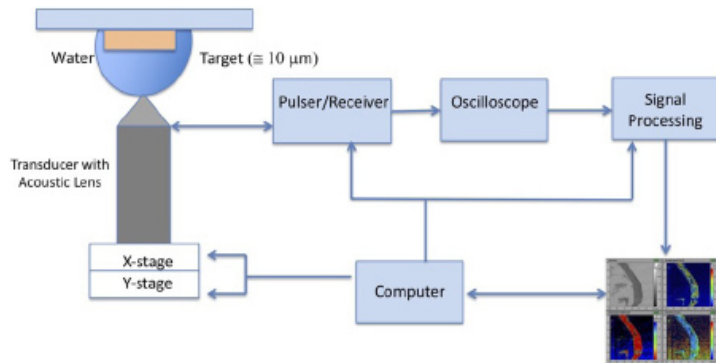
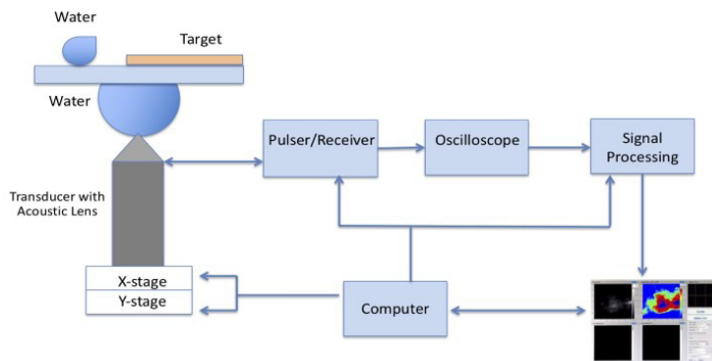**Figure 1:** Schematic of SAM setup in sound speed mode.

Figure 2: Schematic of SAM setup in acoustic impedance mode.

In sound speed mode, the interference of acoustic reflections from the tissue surface (front) and the interface between the tissue and the substrate (rear), as can be seen in Figure 3, is received by the transducer and sound speed distribution within the target is constructed.
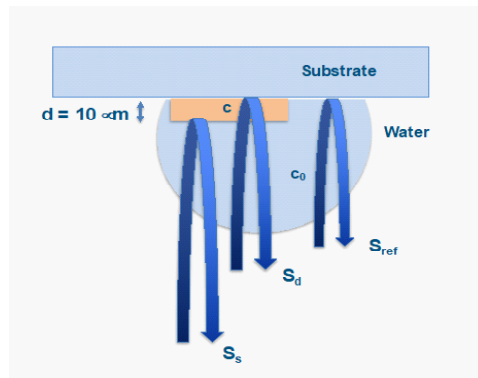

Figure 3: Principle of SAM in sound speed mode. The acoustic waves reflected from the surfaces of distilled water and the tissue are collected by the same transducer and compared for the calculation of the acoustic impedance of the tissue.

The reflected waveform from the specimen has two components, which are reflections from the front and rear sides of the target, and it is not easy to separate these two independent signals. The analysis in frequency domain, by Fourier transforming the waveform, will enable calculation of intensity and phase spectra [28]. The following expressions at any frequency f are derived.

$$2\pi f \times \frac{2d}{c_0} = \phi_{front} \tag{1}$$

$$2\pi f \times 2d \left(\frac{1}{c_0} - \frac{1}{c}\right) = \phi_{rear} \tag{2}$$

where d, c_0, ϕ_front and ϕ rear are target thickness, sound speed of water and phase angles obtained from the front and rear peaks, respectively. The thickness and sound speed at frequency f are calculated as

$$d = \frac{c_0}{4\pi f}\phi_{front} \tag{3}$$
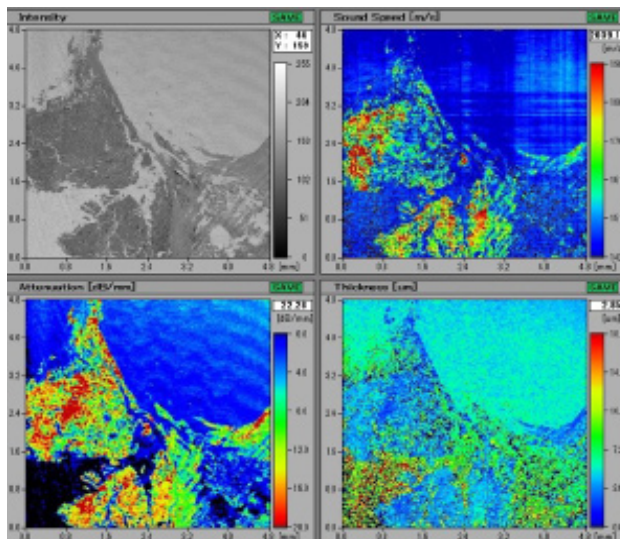
$$d = \frac{c_0}{4\pi f}\phi_{front} \tag{4}$$

Figure 4: SAM images of a fibrocalcific plaque sample. Top left image is the intensity image. Top right image is the sound speed map of the sample. Bottom left image is the attenuation map within the plaque. Bottom right is the thickness map of the sample, indicating an average thickness of 5 μm.

In acoustic impedance mode, image is constructed using the acoustic reflections from both surfaces of the reference (water) and the target cross-section on the substrate (Figure 5). The 2-dimensional distributions indicate different acoustic properties due to the variation of elasticity within the targets.
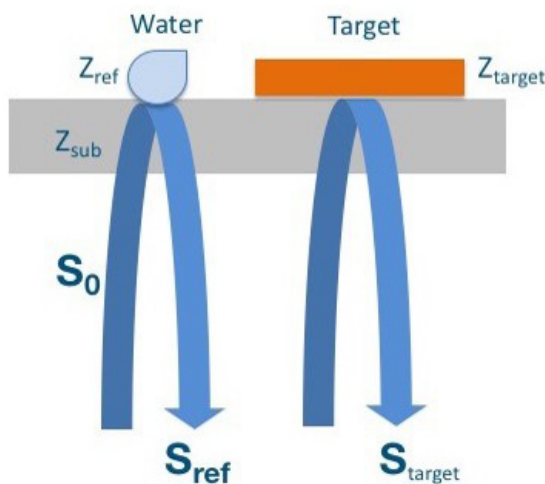

Figure 5: Principle of SAM in acoustic impedance mode. The acoustic waves reflected from the surfaces of distilled water and the tissue are collected by the same transducer and compared for the calculation of the acoustic impedance of the tissue.

SAM in acoustic impedance mode measures the acoustic impedance of the target by comparing the reflected signal from the tissue with the one from the reference. The reflected signal from the reference is

$$S_{ref} = \frac{Z_{ref} - Z_{sub}}{Z_{ref} + Z_{sub}} S_0 \qquad (5)$$

where S_0 is the signal generated by the transducer of SAM, Z_ref is the reference's acoustic impedance (1.50 MRayl) and Z_sub is the substrate's acoustic impedance. The signal reflected by the target is

$$S_{target} = \frac{Z_{target} - Z_{sub}}{Z_{target} + Z_{sub}} S_0 \qquad (6)$$

Consequently, the target's acoustic impedance is calculated as

$$Z_{target} = \frac{1 + \frac{S_{target}}{S_0}}{1 - \frac{S_{target}}{S_0}} Z_{sub} \qquad (7)$$

Figure 6 shows the acoustic impedance map of a fibrocalcific atherosclerotic plaque [30]. This image was constructed using the acoustic reflections from both surfaces of the reference (water) and the plaque cross-section on the polystyrene substrate and operating SAM in acoustic impedance mode. The acoustic impedance distribution indicated different acoustic properties due to the variation of elasticity within the atherosclerotic plaques. The acoustic impedance was determined to be less than 2 MRayl for the collagen-rich areas and greater than 2 MRayl for the calcified areas.
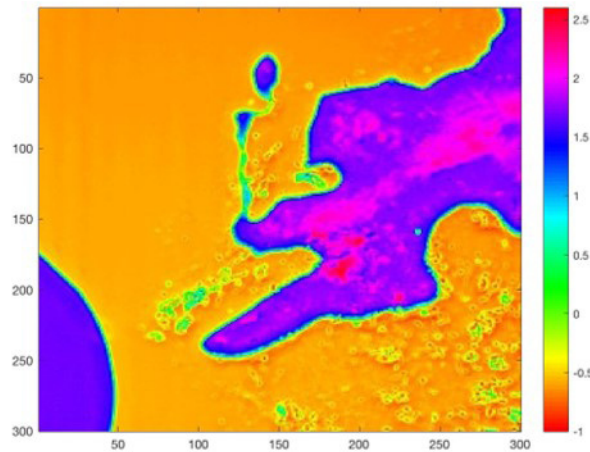

Figure 6: Acoustic impedance map of an atherosclerotic plaque obtained by comparing the reflected ultrasound signals from the surfaces of water (bottom left corner) and the sample. The scanning area is 4.8 mm x 4.8 mm.

4. Photoacoustic Microscopy

Photoacoustic microscopy (PAM) combines optical and ultrasound imaging. In this technique, a pulsed laser, typically, a nano-second laser, excites the tissue and absorbed photons lead to pressure waves via thermoelastic expansion. Ultrasonic transducers capture the emerged pressure waves and produce the map of optical absorbers located within the tissue. Since ultrasonic waves scatter less in biological tissue as opposed to visible portion of electromagnetic spectrum, penetration depth is much better. PAM is named optically resolved

photoacoustic microscopy (OR-PAM), when focused spotsize on the sample determines the resolution of the imaging system. A schematic of OR-PAM is given in **Figure 7**. The sample is scanned with a nano-second laser, which has a suitable wavelength for the excitation of the target under investigation. A transducer is used for the detection of acoustic signals created by the target material. Finally, the maps of samples are constructed. In **Figure 8**, calcific regions with greater acoustic impedance values (**Figure 6**) is also discriminated by PAM.
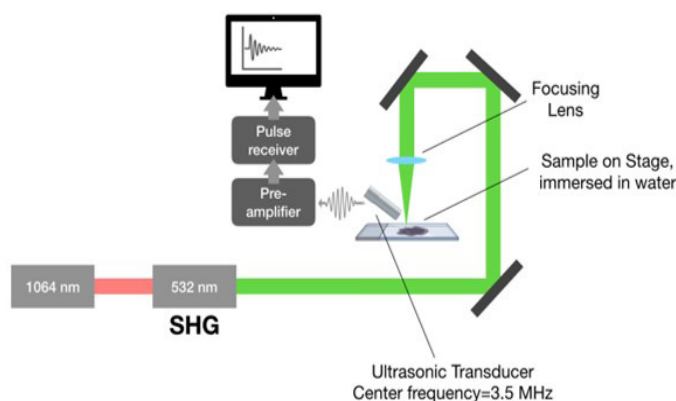

Figure 7: A representative OR-PAM schematic. The sample is scanned with a nano-second laser which is a frequency doubled fiber laser (second harmonic generation-SHG) operating at 532 nm. A transducer with a 3.5 MHz center frequency is used for the detection of acoustic signals.
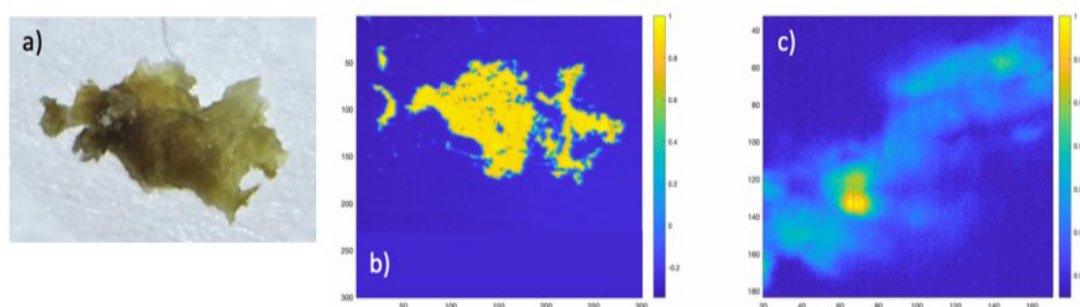

Figure 8: a) Digital image, b) normalized acoustic impedance map, and c) photoacoustic image of the fibrocalcific atherosclerotic human plaque.

5. Conclusions

Here, we discuss the abilities of the acoustic imaging modalities of SAM and PAM, by comparing their capabilities on the determination of plaque components of atherosclerotic fibrocalcific human plaques. The collagen-rich and calcific regions within the plaques are discriminated successfully. SAM and PAM monitor the microcalcifications. SAM provides micrometer resolution in morphology and also mechanical information about the samples. Acoustic impedance maps of the samples show clearly different values in collagen-rich and calcified regions. PAM is also capable of differentiating calcific regions from collagen-rich regions by exhibiting different signals with the chosen excitation source wavelength. Consequently, SAM and PAM seem successful since they are capable of acquiring morphological and chemical information about the plaques simultaneously and usable in clinics. However, for in vivo studies, an intravascular probes, similar to intravascular ultrasound (IVUS) probe, have to be developed.

6. Acknowledgements

7. References

1. Kamiyama N, Okomura Y, Kakee A, Hashimoto H. Investigation of ultrasound image processing to improve perceptibility of microcalcifications. Journal of Medical Ultrasonics. 2008;35:97-105.

2. Hui J, Cao Y, Zhang Y, Kole A, Wang P, Yu G, Eakins G, Sturek M, Chen W, Cheng JX. Real-time intravascular photoacoustic-ultrasound imaging of lipid-laden plaque in human coronary artery at 16 frames per second. Scientific Reports. 2017;7:1417.

3. Zhang J, Yang S, Ji X, Zhou Q, Xing D. Characterization of Lipid-Rich Aortic Plaques by Intravascular Photoacoustic Tomography. Journal of the American College of Cardiology. 2014;64:4.

4. Xu M, Wang L. Photoacoustic imaging in biomedicine. Review of Scientific Instruments. 2006; 77:041101.

5. Zhou Y, Yao J, Wang L. Tutorial on photoacoustic tomography. Journal of Biomedical Optics. 2016;21:061007–061007.

6. Yamazaki R, Ogasawara K, Fujiwara M, Kobayashi K, Saijo Y. Macrophage with Gold Nanorod Visualized by Optical-Resolution and Acoustic-Resolution Photoacoustic Microscopes. In: Conference Proceedings of IEEE Engineering in Medicine and Biology Society. 2015. doi:10.1109/EMBC.2015.7318874

7. Ha S, Tripathy S, Carson A, Lavery LL, Zhang H, Agarwal A, Kotov N, Villanueva FS, Kim K. Multi-target photoacoustic molecular imaging of cardiovascular inflammatory biomarkers using bioconjugated gold nanorods. In: Proceedings of SPIE; 23-25 January 2011; San Francisco. SPIE BIOS; 2011. p. 78991M

8. Miura K, Egawa Y, Moriki T, Mineta H, Harada H, Baba S, Yamamoto S. Microscopic observation of chemical modification in sections using scanning acoustic microscopy. Pathology International. 2015;65(7):355-366.

9. Y Saijo Y, Filho ES, Sasaki H, Yambe T, Tanaka M, Hozumi N, Kobayashi K, Okada N. Ultrasonic tissue characterization of atherosclerosis by a speed-of-sound microscanning system. IEEE Transactions on Ultrasonics Ferroelectrics and Frequency Control. 2007;54(8):1571-1577.

10. Akhtar R, Cruickshank JK, Zhao X, Derby B, Weber T. A pilot study of scanning acoustic microscopy as a tool for measuring arterial stiffness in aortic biopsies. Artery Research. 2016;13:1-5.

11. Y Saijo Y, Hozumi N, Lee C, Nagao M, Kobayashi K, Oakada N, Tanaka N, Filho ES, Sasaki H, Tanaka M, Yambe T. Ultrasonic speed microscopy for imaging of coronary artery. Ultrasonics. 2006;44:e51-e55.

12. Miura K, Katoh H. Structural and histochemical alterations in the aortic valves of elderly patients: a comparative study of aortic stenosis, aortic regurgitation, and normal valves. Biomed Research International. 2016;2016:6125204.

13. Brewin MP, Srodon PD, Greenwald SE, Birch MJ. Carotid atherosclerotic plaque characterization by measurement of ultrasound sound speed in vitro at high frequency, 20 MHz. Ultrasonics. 2014;54:428-441.

14. Saijo Y, Miyakawa T, Sasaki H, Tanaka M, Nitta S. Acoustic properties of aortic aneurysm obtained with scanning acoustic microscopy. Ultrasonics. 2004;42:695-698.

15. Saijo Y, Ohashi T, Sasaki H, Sato M, Jorgensen CS, Nitta S. Application of scanning acoustic microscopy for assessing stress distribution in atherosclerotic plaque. Annals of Biomedical Engineering. 2001;29:1048-1053.

16. Miura K, Nasu H, Yamamoto S. Scanning acoustic microscopy for characterization of neoplastic and inflammatory

lesions of lymph nodes. Scientific Reports. 2013;3:1255.

17. Miura K, Yamamoto S. Pulmonary imaging with a scanning acoustic microscope discriminates speed-of-sound and shows structural characteristics of disease. Laboratory Investigation. 2012;92:1760-1765.

18. Kobayashi K, Yoshida S, Saijo Y, Hozumi N. Acoustic impedance microscopy for biological tissue characterization. Ultrasonics. 2014;54:1922-1928.

19. [19] Hatori K, Saijo Y, Hagiwara Y, Naganuma Y, Igari Kand K, Iikubo M, Kobayashi K, Sasaki K. Acoustic diagnosis device for dentistry. Interface Oral Health Science. 2016;2016:181-201.

20. [20] Strohm EM, Czarnota GJ, Kolios MC. Quantitative measurements of apoptotic cell properties using acoustic microscopy. IEEE Transactions on Ultrasonics Ferroelectrics and Frequency Control. 2010;57(10):2293-2304.

21. Shelke A, Brand S, Kundu T, Bereiter-Hahn J, Blasé C. Mechanical property quantification of endothelial cells using scanning acoustic microscopy. In: Proceedings of SPIE; 11-15 March 2012; San Diego. SPIE; 2012. p. 83481T

22. Brand S, Czarnota GJ, Kolios MC, Weiss EC, Lemor R. Visualization of apoptotic cells using scanning acoustic microscopy and high frequency ultrasound. In: Proceedings of the IEEE Ultrasonics Symposium 2; 18-21 September 2005; Rotterdam. IEEE; 2005. p. 882-885

23. Masugata H, Mizushige K, Senda S, Kinoshita A, Lu X, Sakamoto H, Sakamoto S, Matsuo H. Tissue characterization of myocardial cells by use of high-frequency acoustic microscopy: differential myocyte sound speed and its transmural variation in normal, pressure-overload hypertrophic, and amyloid myocardium. Angiology. 1999;50(10):837-845.

24. Miura K, Yamamoto S. A scanning acoustic microscope discriminates cancer cells in fluid. Scientific Reports. 2015;5:15243.

25. Strohm EM, Kolios MC. Quantifying the ultrasonic properties of cells during apoptosis using time resolved acoustic microscopy. In: IEEE International Ultrasonics Symposium; 20-23 September 2009; Rome. IEEE; 2009. p. 11208710

26. Saijo Y, Sasaki H, Sato M, Nitta S, Tanaka M. Visualization of human umbilical vein endothelial cells by acoustic microscopy. Ultrasonics. 2000;38:396-399.

27. Soon TTK, Chean TW, Yamada H, Takahashi K, Hozumi N, Kobayashi K, Yoshida S. Effects of anticancer drugs on glia-glioma brain tumor model characterized by acoustic impedance microscopy. Japanese Journal of Applied Physics. 2017;56:07JF15.

28. Hozumi N, Yamashita R, Lee CK, Nagao M, Kobayashi K, Saijo Y, Tanaka M, Tanaka N, Ohtsuki S. Time-frequency analysis for pulse driven ultrasonic microscopy for biological tissue characterization. Ultrasonics. 2004;42:717-722.

29. Bilen B, Turker Sener L, Albeniz I, Sezen M, Unlu MB, Ugurlucan M. Determination of Ultrastructural Properties of Human Carotid Atherosclerotic Plaques by Scanning Acoustic Microscopy, Micro-Computer Tomography, Scanning Electron Microscopy and Energy Dispersive X-Ray Spectroscopy. Scientific Reports. 2019;9:679.

30. Bilen B, Gokbulut B, Kafa U, Heves E, Inci MN, Unlu MB. Scanning Acoustic Microscopy and Time-Resolved Fluorescence Spectroscopy for Characterization of Atherosclerotic Plaques. Scientific Reports. 2018;8:14378.